-DRAFT-

Proceedings of the 10th International Pipeline Conference
IPC2014
September 29 - October 3, 2014, Calgary, Alberta, Canada

IPC2014-33225

DESIGN OF THE FULL SCALE EXPERIMENTS FOR THE TESTING OF THE TENSILE STRAIN CAPACITY OF X52 PIPES WITH GIRTH WELD FLAWS UNDER INTERNAL PRESSURE AND TENSILE DISPLACEMENT

Celal Cakiroglu
Department of Civil and Environmental Engineering,
University of Alberta
Edmonton, Alberta, Canada

Samer Adeeb
Department of Civil and Environmental Engineering,
University of Alberta
Edmonton, Alberta, Canada

J. J. Roger Cheng
Department of Civil and Environmental Engineering,
University of Alberta
Edmonton, Alberta, Canada

Millan Sen
Enbridge Pipelines Inc.
Edmonton, Alberta, Canada

ABSTRACT

Pipelines can be subjected to significant amounts of tensile forces due to geotechnical movements like slope instabilities and seismic activities as well as due to frost heave and thaw cycles in arctic regions. The tensile strain capacity (ε_t^{crit}) of pipelines is crucial in the prediction of rupture and loss of containment capability in these load cases. Currently the Oil and Gas Pipeline Systems code CSA Z662-11 [1] contains equations for the prediction of ε_t^{crit} as a function of geometry and material properties of the pipeline. These equations resulted from extensive experimental and numerical studies carried out by Wang et al [2], [3], [4], [5], [6], [7] using curved wide plate tests on pipes having grades X65 and higher. Verstraete et al [8] conducted curved wide plate tests at the University of Ghent which also resulted in tensile strain capacity prediction methods and girth weld flaw acceptability criteria. These criteria are included in the European Pipeline Research Group (EPRG) Tier 2 guidelines. In these methods a pressure correction factor is used to estimate the effect of internal pressure. Further research of Wang et al with full scale pipes having an internal pressure factor of 0.72 also showed that ε_t^{crit} decreases in the presence of internal pressure. There is a recognizable knowledge gap in the literature for understanding the tensile strain capacity of pipes with grades less than X65 as a function of girth weld flaw sizes and the internal pressure.

In this paper the experimental setup for the testing of grade X52 full scale specimens with 12” diameter and ¼” wall thickness is demonstrated. In the scope of this research 8 full scale specimens will be tested and the results will be used to formulate the tensile strain capacity of X52 pipes under internal pressure. The specimens are designed for the simultaneous application of displacement controlled tensile loading and the internal pressure. Finite element analysis is applied in the optimization process for the sizes of end plates and connection elements. Also the lengths of the full scale specimens are determined based on the results from finite element analysis. The appropriate lengths are chosen in such a way that between the location of the girth weld flaw and the end plates uniform strain zones could be obtained. The internal pressure in these experiments is ranging between pressure values causing 80% SMYS and 30% SMYS hoop stress. The end plates and connection elements of the specimens are designed in such a way that the tensile displacement load is applied with an eccentricity of 10% of the pipe diameter with the purpose of increasing the magnitude of tensile strains at the girth weld flaw location.

The results of the first full scale experiment of this research program are presented. The structural response from the experiment is compared to the finite element simulation. The remote strain values of the experiment are found to be higher than the ε_t^{crit} values predicted by the equations in [1].

NOMENCLATURE

ε_t^{crit}	Tensile strain capacity
δ	Apparent crack-tip opening displacement (CTOD) toughness [mm]
η	Ratio of defect height to pipe wall thickness
λ	Ratio of yield strength to tensile strength (Y/T)
ξ	Ratio of defect length to pipe wall thickness
a	Defect height for surface –breaking defect [mm]
$2a$	Defect height for buried defect [mm]
$2c$	Defect length [mm]
t	Pipe wall thickness [mm]
OD	Outer diameter of the pipe
SMYS	Specified minimum yield stress
ν	Poisson' s ratio
E	Modulus of elasticity
σ_h	Hoop stress
σ_l	Longitudinal stress
ε_h	Hoop strain
ε_l	Longitudinal strain
p_i	Internal pressure
CTOD	Crack tip opening displacement

INTRODUCTION

Steel pipelines have proven to be the most efficient form of oil and natural gas transportation from the remote locations of source like the sub-Arctic region of North America to the location of consumption. Due to excessive temperature fluctuations and freezing/thawing cycles of the permafrost significant tensile forces are applied on the pipes. These forces cause longitudinal strains due to differential settlement which can exceed the tensile strain capacity (ε_t^{crit}) of the pipe. Also geotechnical forces caused by slope instability or seismic activity can lead to pipe failure and loss of containment capability due to crack propagation. Girth welds are the parts of a pipeline which are most likely to experience crack propagation and reduced tensile strain capacity because of the high likelihood of welding flaws. In the CSA Z662-11 code [1] girth weld flaws are categorized as surface flaws (Figure 1) and buried flaws. In [1] two sets of equations describe the relationship between girth weld flaw size, material properties and ε_t^{crit} for both of these flaw types. These equations are developed based on the extensive research of Wang et al [2], [3], [4], [5], [6], [7].

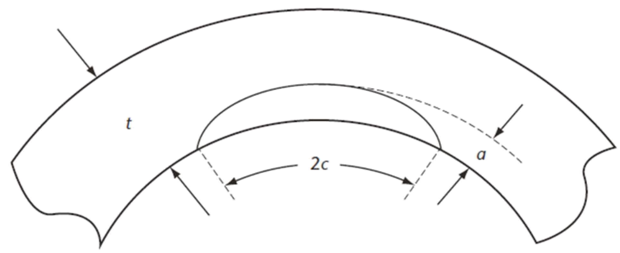

Figure 1: A planar surface-breaking defect in the pipe wall [1]

$$\varepsilon_t^{crit} = \delta^{2.36-1.58\lambda-0.101\xi\eta}(1+16.1\lambda^{-4.45})(-0.157 + 0.239\xi^{-0.241}\eta^{-0.315}) \quad (1)$$

$$\varepsilon_t^{crit} = \varepsilon_t^{crit}(\delta, \xi, \eta, \lambda) \quad (2)$$

In the scope of this paper we are dealing with the effect of surface type girth weld flaws on the tensile strain capacity. In order to investigate this effect, a flaw is machined into the heat effected zone (HAZ) of the pipe since this location has less material strength compared to the girth weld itself and the rest of the pipe base metal.

In our previous work [9] it was found that for the case of surface flaw, the flaw depth has the greatest effect on ε_t^{crit} compared to the other parameters in Eq. (1) and Eq. (2). In this experimental program the variation of ε_t^{crit} with respect to flaw depth ($\eta \cdot t$) and flaw length ($\xi \cdot t$) is investigated for X52 pipe. The study of the effect of internal pressure on ε_t^{crit} is a major component of the research program. The equations currently available in CSA code for the prediction of ε_t^{crit} are developed based on curved wide plate tests. Therefore it is crucial to analyze the variation of ε_t^{crit} at different internal pressure levels. In this paper the experimental setup and the preliminary analyses for different experimental components are elaborated. Also the results of the first full scale experiment are presented.

1. DESIGN OF THE FULL SCALE EXPERIMENT

This section explains the general design process of the full scale specimen as well as the details of the preliminary numerical analysis. Based on the estimated forces acting on the specimen, proper dimensions are determined for the end plates. Also this section describes the test setup and the flaw cutting procedure schematically.

In the scope of this project a total of 8 full scale experiments (Table 1) will be carried out. This paper presents the preparation and results of the first of these experiments. The experimental setup (Figure 14, Figure 16) mainly consists of a 72" long pipe with 12" diameter having a girth weld in its mid-section being tested in an MTS machine under tensile displacement, in the presence of internal pressure and a flaw machined into the heat effected zone.

Table 1: Test matrix

Test number	Specimen Length	Internal pressure (% SMYS)	Flaw length [mm]	Flaw depth [mm]
1	72”	80	50	1.7
2	72”	10	50	1.7
3	72”	80	50	3.4
4	48”	30	50	3.4
5	72”	80	150	1.7
6	48”	10	150	1.7
7	48”	80	150	3.4
8	48”	30	150	3.4

1.1 PRELIMINARY FINITE ELEMENT ANALYSIS

In this section the details of the preliminary finite element model of the full scale specimen are elaborated. This model is used for the estimation of the expected forces that the end plates undergo during the experiment. For this purpose 12.7 MPa (80% SMYS hoop stress) internal pressure as well as eccentric tensile displacement are applied in consecutive load steps in the simulation software “Abaqus”. In order to simulate the effect of the girth weld flaw on the stress distribution, the element thickness is reduced to 75% of the pipe wall thickness at the girth weld location aligned with the tongue which is denoted as “Flaw” in Figure 2.

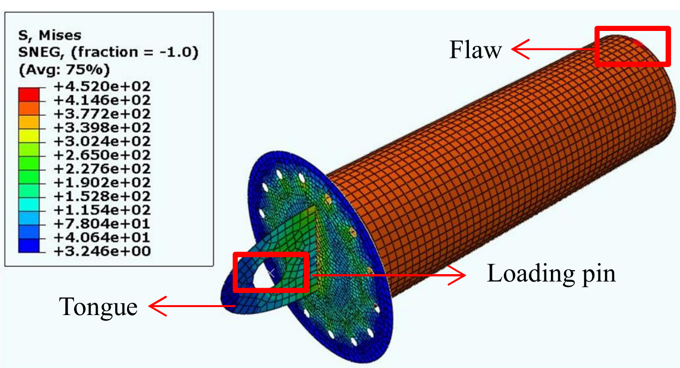

Figure 2: Distribution of the von Mises stress on the finite element model

The visualization of the von Mises stress distribution for an applied internal pressure of 12.7 MPa and 30 mm tensile displacement are shown in Figure 2. In this finite element model the end plate which is welded to the pipe base metal and the fixture plate which has the tongue part (Figure 14) are modeled as a single plate having 70 mm thickness. However in the experiment these two plates are connected to each other with 14 bolts. The holes on the end plate in Figure 2 represent the locations of these bolt holes. The material properties listed in Table 2 are used throughout the finite element model.

Table 2: Material properties of the pipe base metal and the geometric parameters

Modulus of Elasticity [MPa]	201530
SMYS [MPa]	357
Ultimate strength [MPa]	452
Pipe outer diameter (OD) [mm]	324
Pipe wall thickness (t) [mm]	7
Maximum high-low misalignment [mm]	0.896
Pipe half-length	3OD

In order to determine a proper wall thickness value to be used in the numerical models, the pipe wall thickness is measured in random locations of the pipe. In total 53 measurements are made. The outlier data which lies 3 standard deviations or more away from the average value is replaced with the average wall thickness. The histogram in Figure 3 shows the frequency of different wall thickness ranges.

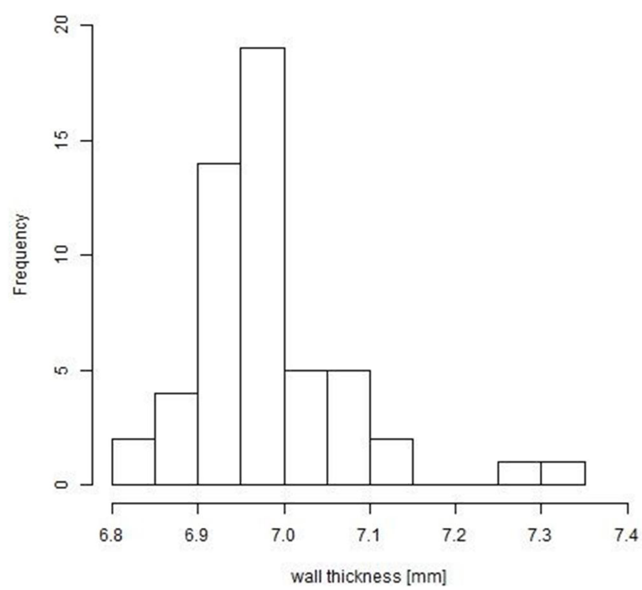

Figure 3: Frequency distribution of the wall thickness

According to this histogram a substantial part of the wall thickness measurements fall into the range between 6.9 mm and 7.0 mm. Therefore the average of these two values (6.95 mm) is used as wall thickness in the finite element analysis.
After the application of the 12.7 MPa internal pressure in the first load step, in the second load step 85 mm displacement is applied on a rigid point in the middle of the tongue hole in a direction parallel to the pipe longitudinal axis. In the experimental setup this tongue slides into a yoke and a pin connects the tongue to the yoke building a so called pin- yoke assembly (Figure 4). Therefore in the consecutive parts of this text the rigid point at the center of the tongue hole is referred to as the loading pin.

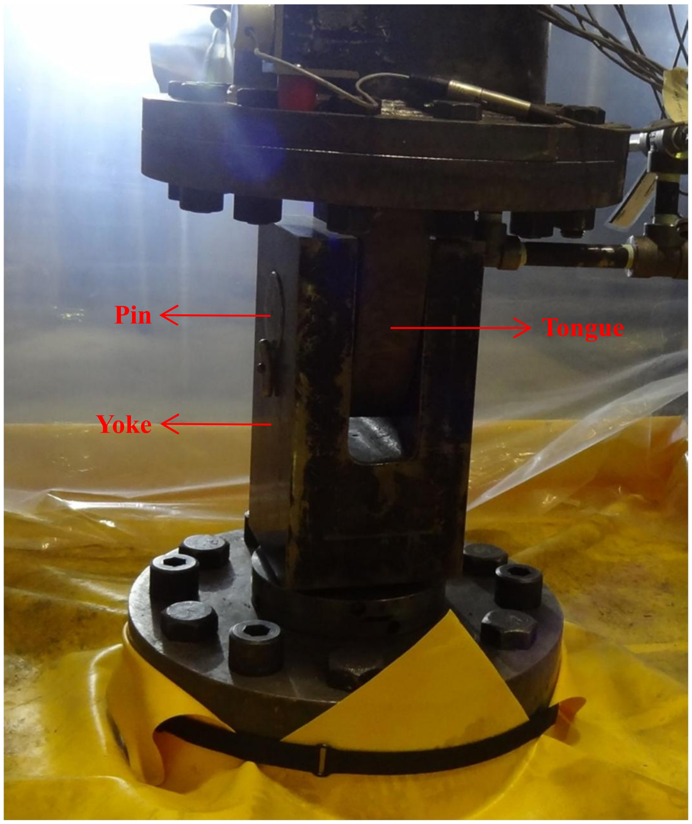

Figure 4: Pin-yoke assembly connected to the tongue

In order to transfer the forces to the internal surface of the tongue hole, in the Abaqus finite element model a rigid point tie constraint is defined between the loading pin and the tongue internal surface. Similarly another rigid point is defined at the center of the end plate and this rigid point is connected to the internal surfaces of all 14 bolt holes using tie constraints. In this way the effect of applying longitudinal displacement to the loading pin on the bolt holes and the end plate is simulated.

Due to the eccentricity of the tensile displacement (0.1 OD) the end plate rotates throughout the experiment. In order to simulate the effect of this rotation all degrees of freedom of the end plate is constrained except the rotation and axial displacement.

It can be observed in Figure 5 that starting from an applied displacement of 73 mm, the shapes of the elements in the vicinity of the flaw become highly distorted. At this same amount of displacement also the reaction force at the loading pin starts to drop significantly (Figure 6) which can be interpreted as an indication of material failure.

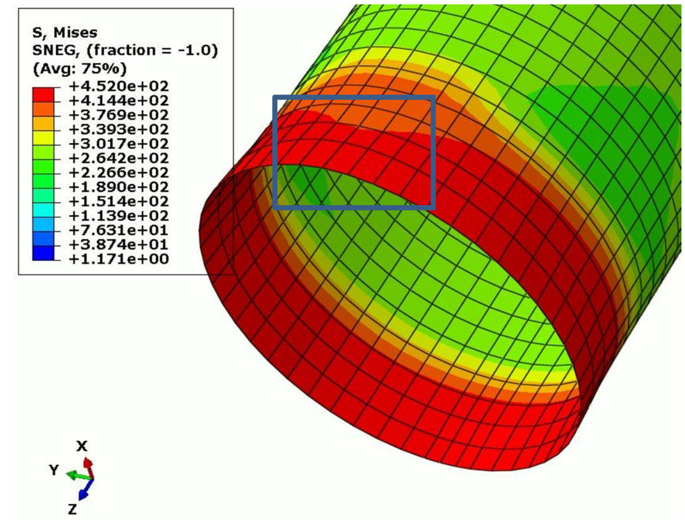

Figure 5: Distorted elements at the flaw location

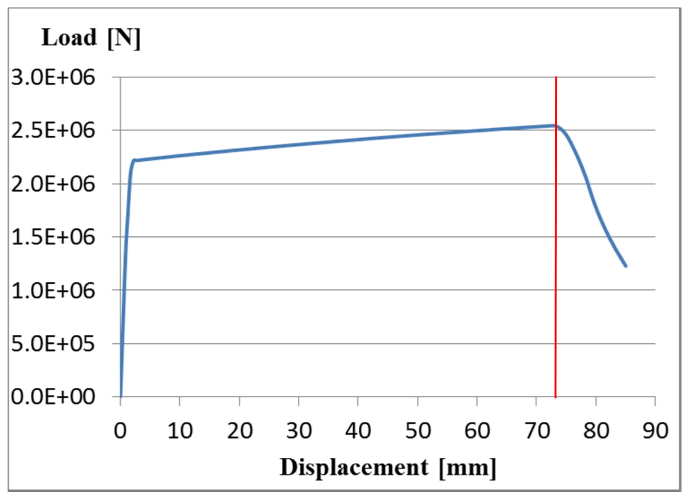

Figure 6: Reaction force - displacement relationship from the numerical model

1.2 END PLATE DESIGN

The end plate is designed based on the results of the preliminary finite element simulation. In the geometry optimization process a feedback control approach is adopted as illustrated in Figure 7.

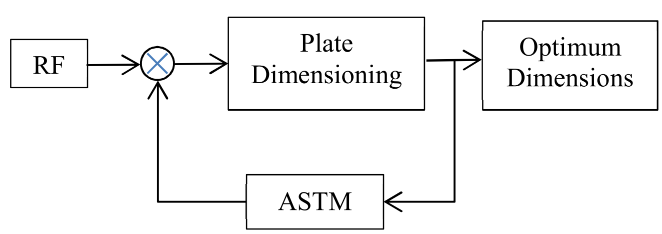

Figure 7: Block diagram showing the process of the end plate geometry optimization

In Figure 7, RF denotes the reaction force at the loading pin. The total tensile force applied on the end plate is used to design a bolted connection between the pipe end plate and another connection plate. For this purpose the maximum reaction force from Figure 6 is multiplied with a safety factor yielding a magnified applied force of 4029 kN. Using this RF value the number and diameter of bolt holes are varied until the safety criteria of the ASTM code A490 were met.

1.3 HIGH - LOW MISALIGNMENT AT THE GIRTH WELD

In the process of creating the high-low misalignment profile of the full-scale specimens a 3D laser scanner is utilized. The surface geometry which is captured by the laser scanner is analyzed using the reverse engineering software Geomagic. In this procedure the 3D surface geometry of the girth weld location is compared with a perfect cylinder having the same nominal diameter as the scanned pipe. This nominal diameter value can be obtained in Geomagic as the diameter of the best fit cylinder to the scanned pipe surface. Once the scanned girth weld area and the imported perfect cylinder are overlapped, the 3D comparison algorithm of Geomagic created a colour map (Figure 8) which shows the deviation of the scanned surface from the perfect cylinder in millimeters at each point of the scanned surface. In the colour map of Figure 8 shades of green and blue indicate the scanned surface being underneath the surface of the perfect cylinder and the shades of yellow and red indicate the scanned pipe surface being over the perfect cylinder surface. This colour convention can be clearly recognized from the colour of the girth weld location. This location has a dark red colour since the girth weld middle line has substantially greater diameter than the perfect cylinder.

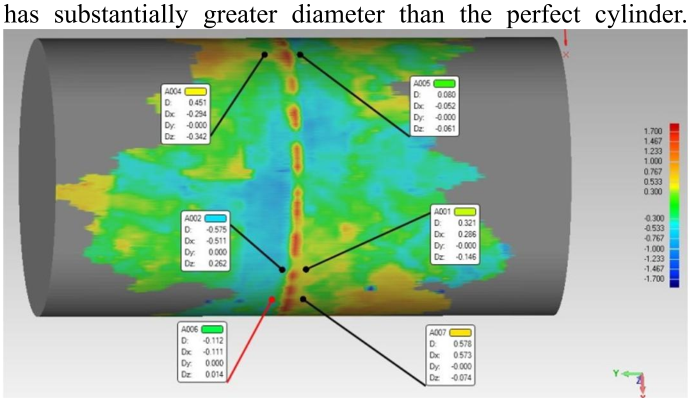

Figure 8: Determination of the maximum high-low misalignment

By observing the colour map of Figure 8, three locations of major deviation could be identified. The annotations in Figure 8 show the deviations of the scanned surface from the perfect cylinder on both sides of the girth weld at these major deviation zones. In these annotations the letters D_x, D_y, D_z show the deviations between two surfaces in x, y and z directions respectively and the letter D shows the magnitude of the deviation at a certain point. The minus signs indicate that the scanned surface is beneath the perfect cylinder surface and positive deviation indicates that the scanned surface is over the perfect cylinder surface. Based on the deviation measurements at the three major deviation zones it was concluded that the maximum high – low misalignment was 0.896 mm in magnitude.

1.4 MACHINING THE GIRTH WELD FLAW

For the first experiment in the test matrix (Table 1), a flaw of 1.7 mm depth and 50 mm circumferential length is machined in two stages using blades of two different thicknesses. This flaw depth corresponds to 25% of the total pipe wall thickness (t). In the first stage the flaw is initiated using a jewellery blade of 0.012” thickness and cut up to a depth of 1.0 mm. In the second stage the blade is replaced with one of 0.006” thickness and the remaining 0.7 mm depth of the flaw is cut. Before starting to cut the flaw it is checked with an L-shaped ruler that the pipe surface is perfectly perpendicular to the blade. Afterwards the first 1.0 mm of the flaw is cut in 20 steps. In each step the depth of the flaw is increased 0.05 mm. In order to cut the flaw in circumferential direction, the pipe is rotated 50 mm using the rollers of the pipe stand in the opposite direction of the rotation direction of the blade.

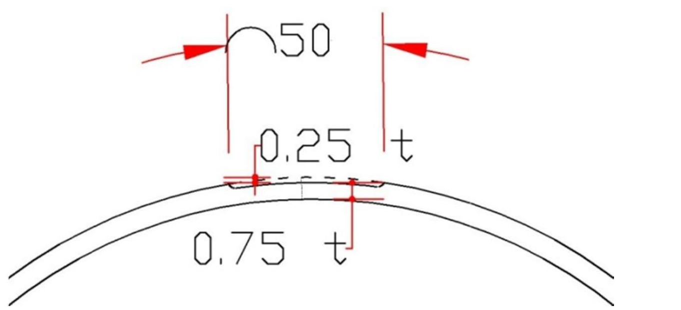

Figure 9: Flaw dimensions (circumferential) [mm]

The flaw machining equipment (Figure 11) consists of an x-y table (G1), an air driven motor which rotates the blade (G2), dial indicators showing the parallel to the pipe (G3) and perpendicular to the pipe (G4) position of the x-y table and a steel block (G5) clamped with the x-y table and holding the blade. The two red magnets on the pipe indicate the starting and ending points of the flaw in the circumferential direction. The depth of the flaw is controlled with the help of dial indicators (Figure 11) in the directions parallel (G1) and perpendicular (G2) to the pipe. The main function of the dial indicator G1 is to adjust the alignment of the blade in the direction parallel to the pipe during the process of replacing the 0.012” thick blade with the 0.006” one. In this process after the replacement of the new blade, the x-y table has to move to the left side 0.003” such that the blade stays aligned with the mid-line of the flaw as shown on the right hand side profile in Figure 10.

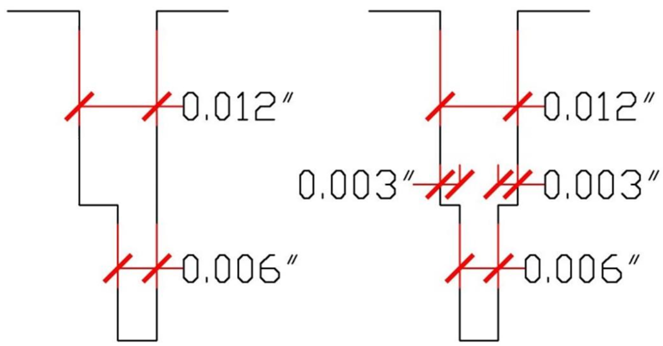

Figure 10: Flaw dimensions (depth), undesired (left), desired (right)

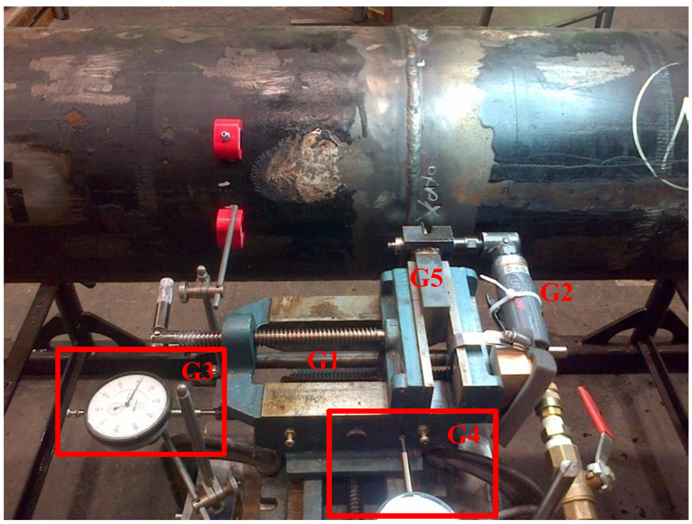

Figure 11: Flaw machining setup

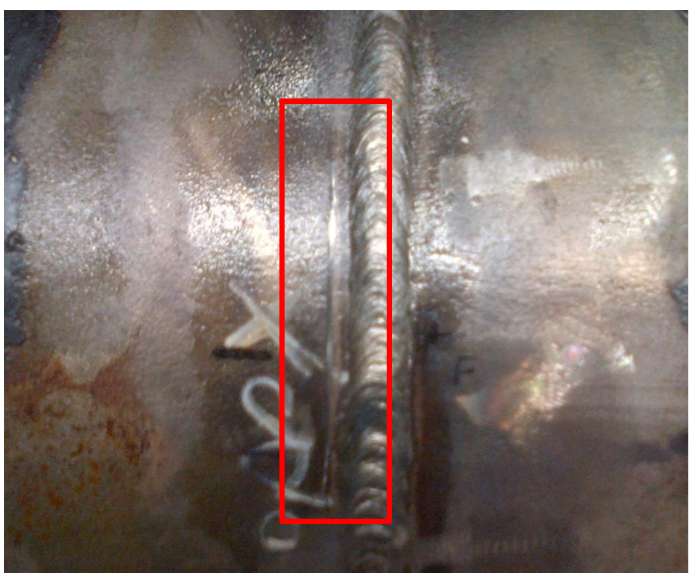

Figure 12: Flaw of 50 mm length and 1.7 mm depth machined into the heat affected zone

2. PREPARATION OF THE FULL SCALE SPECIMEN

In this section the details of the data measurement methods are explained. The main source of information in these tests is the measured strain and internal pressure data as well as the reaction force and displacement measured by the MTS machine. For the collection of strain data strain gauges and digital image correlation techniques are utilized. Also clinometers attached to the top and bottom end plates measured the rotation of end plates throughout the test. This rotation was caused by the eccentricity of the applied load.

2.1 POSITIONING OF THE STRAIN GAUGES

The strain gauges are positioned such that the longitudinal strain values could be measured at the remote strain locations (1 OD away from end plates) as well as in the vicinity of the girth weld flaw. Also the hoop stress is measured in the mid-sections of each side of the pipe with circumferential strain gauges. Due to the eccentricity of the applied displacement the strain values were expected to differ along the circumference of the pipe. Positive longitudinal strain values were expected at the side of the pipe aligned with the flaw whereas compressive strain was expected on the opposite side. On the other hand the exact transition profile from tensile strain to compressive strain along the pipe circumference should be measured. For this purpose the pipe circumference is divided into four quarters (Figure 13) and at each quarter strain gauges are installed.

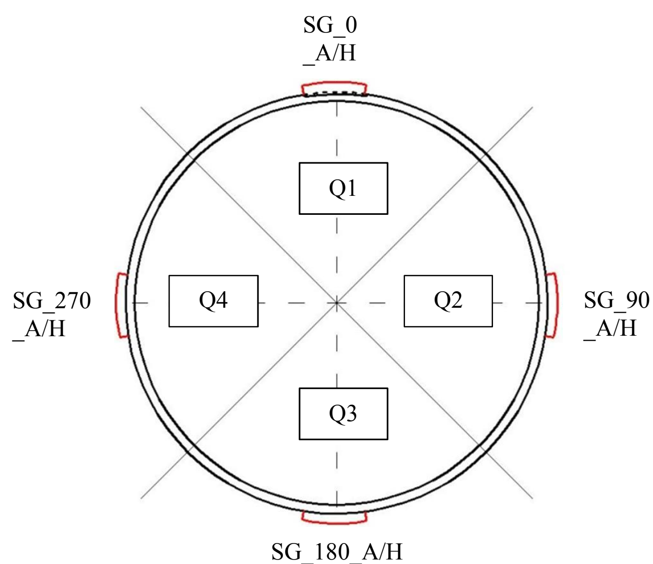

Figure 13: Strain gauge positions around the pipe circumference

These quarters are denoted with Q1 to Q4. The red lines on the pipe surface in the middle of each quarter shows the location of a strain gauge. These lines are separated 90 degrees from each other and are denoted according to their angular distance from the flaw. Also the last letter in each strain gauge name indicates the direction of the strain gauge. For example SG_0_A is the strain gauge which is aligned with the flaw and measures the axial (longitudinal) strain. Similarly SG_90_H is the strain gauge which is located in a clockwise direction 90 degrees away from the flaw and measures the hoop strain at the side of the pipe. In the strain gauge setup the gauges 180 degrees away from the flaw are on the compression side of the pipe and expected to measure compressive strains whereas the gauges 0 degrees away from the flaw are measuring tensile strain values. The main function of the hoop strain gauges is to measure the circumferential expansion of the pipe due to the increasing internal pressure. However the main purpose of these experiments is to investigate the axial tensile strain capacity of the specimens. Therefore hoop strain gauges are applied only at the mid-sections of the pipe.

In order to capture the remote strain, also the gauge setup of Figure 13 is applied although this time the hoop strain gauges are omitted. For this purpose axial strain gauges are installed on the top side of the pipe 1OD away from the end plate. At the bottom side of the pipe the remote strain is captured using digital image correlation. The location of the remote strain is in compliance with the definition of remote strain in [2].

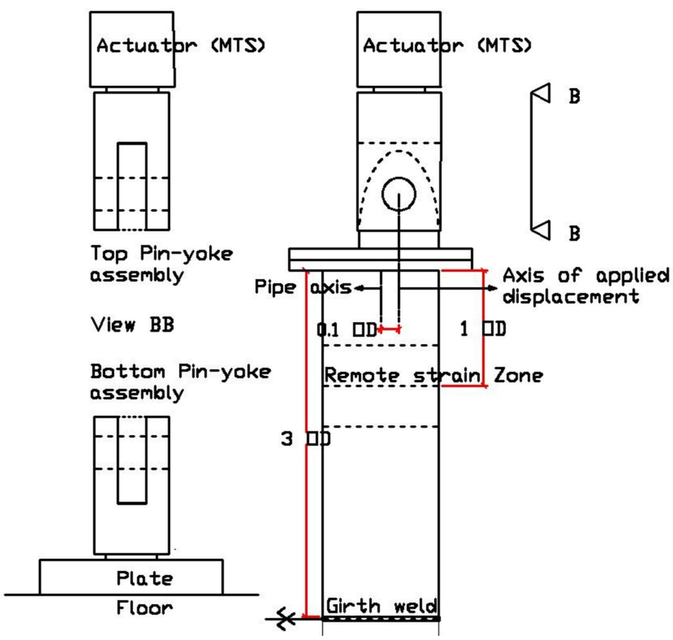

Figure 14: Setup of the experiment

The amount of eccentricity of the applied displacement (0.1 OD) as well as the remote strain location can be seen in Figure 14. The amount of eccentricity of the tongue pieces is identical on both sides of the pipe. Also the pipe lengths on both sides of the girth weld are identical. Using this symmetry, only half of the specimen is shown in Figure 14.

On both ends of the pipe there are fixture plates with tongue pieces. The fixture plates are connected to the end plates with bolts of 1” diameter. These bolts are pre-tensioned before the test using an impact wrench such that any elongation of the bolts due to the applied displacement is excluded from the test results. The tongues are attached to the end plates with fillet welds and have circular holes in them with diameters slightly larger than that of the pin. Also the thickness of the tongue is slightly less than the width of the opening of the yoke. In this way the pin can slide into the tongue once it is inside the yoke, building a pin-yoke assembly (Figure 14). The pin yoke assembly at the top side of the specimen is threaded into the actuator of the MTS machine which applies the displacement. At the bottom side the pipe is connected to the floor with another pin- yoke assembly which is threaded into a plate and this plate is bolted to the floor.

2.2 APPLYING THE INTERNAL PRESSURE

In order to apply the internal pressure, the pipe is filled with water from a hole at the bottom end plate. Another hole at the upper end plate provides an air outlet so that no air is trapped inside the pipe during the tests. This air outlet is closed with a ball valve once the pipe is filled with water. An air driven pneumatic pump with a pressure capacity of 9800 psi is connected between the bottom end plate and the municipal water supply. Also an automatic pressure relieve valve is connected to the water inlet of the bottom end plate which would release water as soon as the internal pressure exceeds the desired value (1700 psi). This is the internal pressure value which corresponds to 80% SMYS hoop stress.

Figure 15: Air -driven pneumatic pump

2.3 MEASURING THE BENDED PROFILE OF THE SPECIMEN

Due to the eccentricity of the applied displacement, the initially straight pipe axis became curved during the experiment. In order to measure the development of this curvature, cable transducers are connected to the pipe at five different locations in the longitudinal direction. For this purpose an I – profiled steel column is placed approximately 1 m away from the pipe. The steel column and cable transducers are located on the side of the pipe which bends in compression. The cable transducers are connected to the steel column with magnets (Figure 16). In order to connect the cables to the pipe, nuts are glued on the pipe surface using epoxy and eye bolts are screwed into these nuts. The loops of the eye bolts are connected to the cables of the transducers using strings after pulling the cables about 6”.

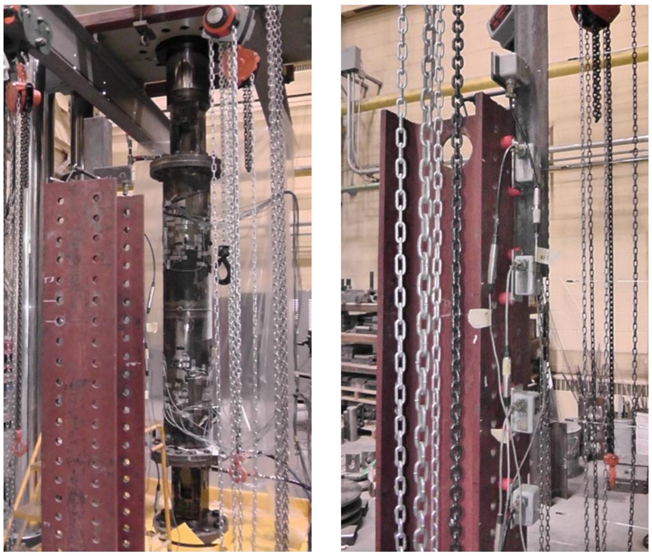

Figure 16: Steel column and cable transducers

3. FULL SCALE TESTING PROCEDURE AND ITS RESULTS

In this section the procedure of testing the specimen is explained. Afterwards the load –displacement response of the first full scale specimen is presented and compared to the response predicted by the finite element analysis. The strain measurements of four different strain gauges at the remote strain zone are illustrated. The measured values of the hoop strain at the mid-section of the top side of the pipe is compared with the theoretical hoop strain values during the process of increasing the internal pressure.

Before applying any displacement to the specimen, the internal pressure is increased to 1700 psi in 200 psi increments. During the pressurization process the motion of the pipe in axial direction was unconstrained so that the axial force was zero throughout pressurization.

Once the internal pressure of 1700 psi was reached, the displacement was applied in a monotonic way at a rate of 0.2 mm/min up to a total displacement of 14.7 mm (1655 kN reaction force). This amount of displacement caused the pipe to reach its elastic limit.

Figure 17: Flaw after rupture

Since after the elastic limit the pipe is expected to exhibit more ductile behaviour, at this point the rate of applied displacement is doubled to 0.4 mm/min. In the nonlinear global response zone the rate of displacement was doubled two more times at 26.3 mm (1890 kN reaction force) and 50mm (2200 kN reaction force) total displacements up to a rate of 1.5 mm/min. Throughout the test the measurements are recorded every 10^{th} second. At a total axial displacement of 62.22 mm and a reaction force of 2339.4 kN the pipe burst at the flaw location due to crack propagation. Figure 17 shows the crack opening after the rupture. After the rupture the pipe was unloaded and a permanent displacement of 52 mm was observed.

3.1 COMPARISON WITH THE FINITE ELEMENT ANALYSIS

The development of the reaction force at the loading pin during the entire experiment is compared to the result of the finite element analysis in Figure 18.

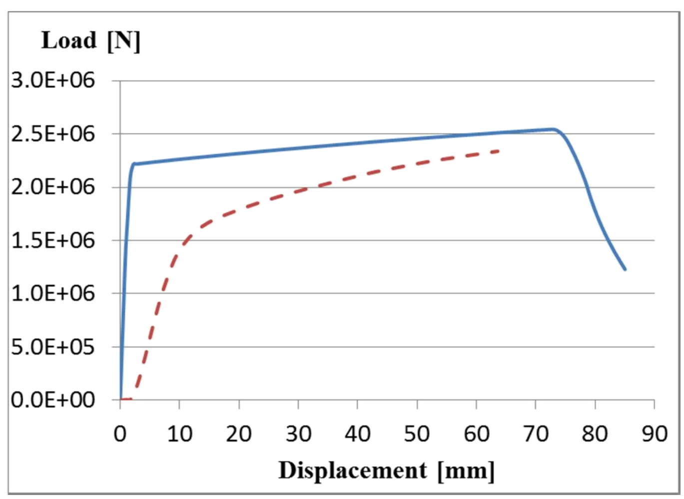

Figure 18: Variation of the reaction force during the experiment (dashed) and in the finite element model (solid)

It can be observed that the maximum load recorded before rupture (2339.4 kN) is fairly close to the numerically predicted maximum load carrying capacity of the pipe (2540 kN). The main source of difference between the two response curves in Figure 18 is the absence of the longitudinal tensile effect of the internal pressure in the numerical model. Also in the numerical model the effect of stress intensity at the crack tip was ignored. In the actual experiment this strass intensity lead to a rapid crack propagation and fracture once the critical strain level was reached. Due to this crack propagation effect also the pipe failure takes place earlier in the experiment by an applied displacement of 63.6 mm. Whereas the finite element model predicts the structural failure at 73.3 mm applied displacement. The rapid crack growth towards the end of the experiment can also be observed from the development of the crack tip opening displacement (CTOD). To have an approximate visualization of this parameter the variation of the displacement between two points on both sides of the flaw, initially 12.11 mm away from each other, is visualized using digital image correlation (Figure 19). This visualization shows the rapid increase in the crack growth rate starting from an applied displacement of about 50 mm which leads to the rupture of the flaw earlier than predicted by the finite element analysis.

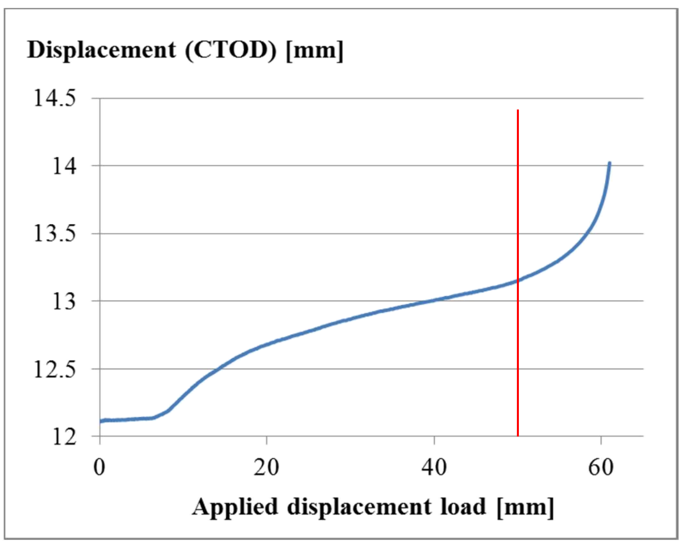

Figure 19: Variation of CTOD with respect to displacement

3.2 REMOTE STRAIN MEASUREMENTS

The remote strain is measured 1OD away from the end plate with four different axial strain gauges with 90 degrees angular intervals (Figure 20).

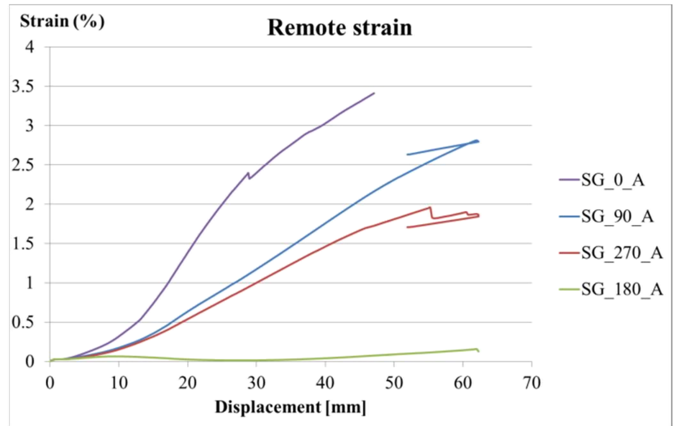

Figure 20: Strain variation at the uniform strain zone

The strain gauges which measured the remote strain are denoted in Figure 20 according to the same naming convention as described in section 2.1. In this graph the green curve represents the strain variation at the opposite side of the flaw. The strain values measured by this strain gauge are negligible compared to the rest of the gauges. Therefore this curve is not considered in the computation of the average remote strain. The strain values of the three other strain gauges before rupture are 3.41%, 2.16% and 1.73% which yields an average remote strain of 2.43%.

3.3 COMPARISON OF THEORETICAL AND EXPERIMENTAL HOOP STRAIN VALUES

Under the assumptions of a plane stress condition and isotropic material behaviour, the hoop strain (ε_h) can be expressed as follows:

$$\varepsilon_h = \frac{1}{E}(\sigma_h - \nu\sigma_l) \tag{3.3.1}$$

Using the definition of σ_h(hoop stress) and σ_l (longitudinal stress) as functions of p_i(internal pressure), OD and t, equation (3.3.1) becomes

$$\varepsilon_h = \frac{1}{E}\left(\frac{p_i \cdot OD}{2t} - \nu\frac{p_i \cdot OD}{4t}\right) \tag{3.3.2}$$

Using (3.3.2), the theoretical hoop strain values and their differences from the experimental values at every internal pressure increment are tabulated in Table 3.

Table 3: Comparison of theoretical and experimental hoop strain values

Internal pressure [psi]	Theoretical hoop strain	Experimental hoop strain	Difference (%)
200	0.000129	0.000128	0.4
400	0.000257	0.000258	0.38
600	0.000386	0.000389	0.9
800	0.000514	0.000521	1.35
1000	0.000643	0.000654	1.78
1200	0.000772	0.000790	2.46
1400	0.000900	0.000925	2.83
1700	0.00109	0.00113	3.45

In Table 3 the experimental hoop strain value is calculated taking the average of four strain gauge measurements in hoop direction at the mid-section of the top side of the pipe. The increase in the difference between theoretical and experimental strain values with increasing internal pressure stems from the fact that as the strain values increase, the validity of the plane stress assumption decreases. Nevertheless a maximum difference of 3.45 % between the measured and theoretical hoop strain values verifies the reliability of the measurements.

3.4 MEASUREMENTS OF THE PIPE AXIS CURVATURE

During the entire experiment the deviation of the pipe axis from a straight line is measured using cable transducers. The recorded deviations at the mid-section of the pipe (Cable Middle), and 1OD away from the end plates (Cable A-1/3, Cable B-1/3) are shown in Figure 21. According to this graph, throughout the experiment, higher deviation values are observed at the top side of the pipe (Cable B-1/3) compared to the bottom side (Cable A-1/3) while in the mid-section the greatest deviation values are observed.

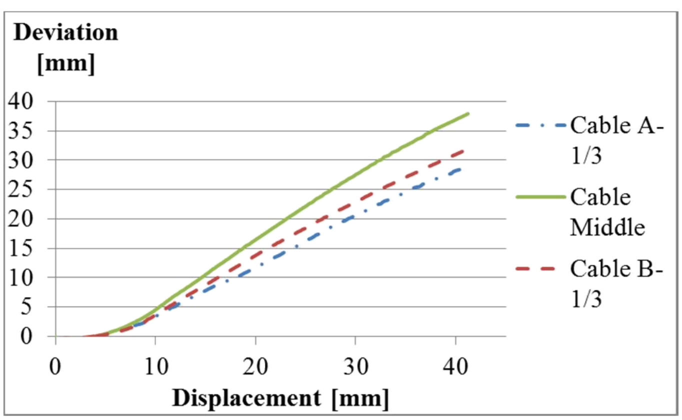

Figure 21: Deviation of the pipe axis from a straight line

4. DISCUSSION AND CONCLUSIONS

In the strain based design of pipelines the presence of possible girth weld defects plays a significant role. Extensive research is done in the recent years in order to better understand the effect of different crack sizes in the vicinity of girth welds on the tensile strain carrying capacity of pipelines. Girth weld locations constitute one of the relatively weaker parts of the pipeline structure. This weakness is mainly due to the presence of heat affected zones around the girth weld. The research projects conducted to date mainly investigated the tensile behaviour of high strength steel pipes of grades X65 and higher. These research projects involved not only testing of curved wide plates cut out of line pipes but also testing of full scale specimens in the presence of internal pressure. The results of these experiments combined with parametric finite element analyses provided valuable insight in the estimation of the tensile strain capacity of high strength steel pipes. These results are used in order to formulate the strain response of high strength steel pipes in the presence of girth weld flaws as a function of pipe material properties, pipe geometry and girth weld flaw size. Currently closed form equations are available in the CSA code for the design of pipeline systems (Z662-11), which can provide accurate predictions for the estimation of the tensile strain capacity of steel pipes having steel grade higher than X65.

Although equations for the prediction of the tensile strain capacity of steel pipes are available in the CSA code, they are not applicable to pipes with steel grade X52. Also the effect of internal pressure is not included in these closed form equations. This paper addresses the current knowledge gap in the prediction of the tensile strain capacity of X52 pipes in the presence of internal pressure. For this purpose a full scale test was carried out at the University of Alberta which involves the testing of a 6OD long pressurized X52 pipe under eccentric displacement controlled loading. In this paper the preparation process of this full scale tensile strain experiment is elaborated. Also the results of the full scale test of the specimen is presented based on both experimental data and finite element analysis. It was found that the X52 pipe with a crack of 50 mm length and 0.25t depth is capable of undergoing about 2.43% longitudinal strain before rupture occurs. On the other hand using the currently available tensile strain equations for this type of pipe would yield an estimated ε_t^{crit} of 0.725% indicating that the code equation is highly conservative when applied to this pipe and crack configuration. More research is thus required in order to formulate the tensile strain response of X52 pipes with high ductility.

REFERENCES

[1] CSA Z662-11; Oil and gas pipeline systems - Sixth Edition; Update No. 1: January 2012

[2] Wang Y-Y.,et al (2011); "Second Generation Models for Strain-Based Design. Contract PR-ABD-1-Project 2. Final Approved Report Prepared for the Design, Materials and

Construction Technical Committee of Pipeline Research Council International, (PRCI) Inc.
[3] Wang, Y-Y., Cheng W., Horsley D. (2004); "Tensile Strain Limits of Buried Defects in Pipeline Girth Welds" Proceedings of IPC2004, International Pipeline Conference, IPC2004-524
[4] Wang, Y-Y., Chen, Y. (2005); "Reliability Based Strain Design" Gas Research Institute Report 04/0146. Des Plaines, IL.
[5] Wang Y-Y., Cheng, W. (2004); "Guidelines on Tensile Strain Limits" Gas Research Institute Report 04/0030. Des Plaines, IL.
[6] Wang Y-Y., et al (2004); "Tensile Strain Limits of Girth Welds with Surface-Breaking Defects, Part 1 – An Analytical Framework" Proceedings of the 4th International Conference on Pipeline Technology, 235—249
[7] Wang Y-Y., et al (2004); "Tensile Strain Limits of Girth Welds with Surface-Breaking Defects, Part 2 – Experimental Correlation and Validation" Proceedings of the 4th International Conference on Pipeline Technology, 251 – 266
[8] Verstraete M., De Waele W., Denys R., Hertele S.(2012); "Comparison of Pipeline Girth Weld Defect Acceptance at the Onset of Yielding According to CSA Z662 and EPRG Guidelines" Proceedings of the 9th International Pipeline Conference IPC 2012-90593
[9] Cakiroglu C., Duke K., El-Rich M., Adeeb S., Cheng J.J.R., Sen M.(2012); "Influence of Girth Weld Flaw and Pipe Parameters on the Critical Longitudinal Strain of Steel Pipes" Proceedings of the 9th International Pipeline Conference IPC 2012-90736
[10] Wang Y-Y., Liu M. (2010); "Toughness Considerations for Strain Based Design" Proceedings of the 8th International Pipeline Conference, IPC2010-31385